Bulletin of Electrical Engineering and Informatics
Vol. 15, No. 3, June 2026, pp. 1956∼1971
ISSN: 2302-9285, DOI: 10.11591/eei.v15i3.10904

AC and DC power transfer optimization research using numerical models for wireless heavy-duty EV charging

Mustafa Karavuş[1,2], Ahmet Arif Ergin[3], Gulten Polat[4], Bünyamin Eşiyok[1]
[1]Department of Electrical and Electronics Engineering, Faculty of Engineering, Yeditepe University, Istanbul, Turkey
[2]TEMSA Skoda Sabancı Ulaşım SAN.TİC.A.Ş, Istanbul, Turkey
[3]Department of Electrical and Electronics Engineering, Faculty of Engineering, Bahcesehir University, Istanbul, Turkey
[4]Department of Civil Engineering, Faculty of Engineering, Yeditepe University, Istanbul, Turkey

Article Info

Article history:

Received Jun 24, 2025
Revised Mar 16, 2026
Accepted Apr 1, 2026

Keywords:

8-switch inverter
AC/DC topologies
Efficiency and sensitivity analysis
Heavy-duty electric vehicles
MATLAB/Simulink
Runge-Kutta method
Wireless power transfer

ABSTRACT

Wireless power transfer (WPT) can enable automated charging of heavy-duty electric vehicles (HDEVs), where high power levels require high efficiency and stable operation. This paper compares AC- and DC-based WPT architectures for the TEMSA LD SB E bus using MATLAB/Simulink simulations. The analysis is conducted at three operating frequencies (80, 85, and 90 kHz) and for coupling coefficients ranging from 0.10 to 0.90 with 0.10 increments. The AC system uses an eight-switch resonant inverter, whereas the DC system employs a direct DC/DC converter. Transient behavior is solved using a fourth-order Runge–Kutta scheme, and electromagnetic interactions are verified via finite-element analysis (FEM). Peak efficiencies of 96.10% (AC) and 97.44% (DC) are achieved at 85 kHz and a coupling coefficient of 0.90. Normalized sensitivity indices and linear regression identify coupling and frequency as dominant factors, while the DC architecture exhibits reduced sensitivity. The results provide quantitative guidance for designing reliable high-power WPT chargers for commercial fleets.

This is an open access article under the CC BY-SA license.

Corresponding Author:

Mustafa Karavuş
Department of Electrical and Electronics Engineering, Faculty of Engineering, Yeditepe University
Istanbul, Turkey
Email: mustafa.karavus@std.yeditepe.edu.tr

1. INTRODUCTION

Wireless power transfer (WPT) has emerged as a promising technology for charging electric vehicles (EVs), offering increased convenience and reduced reliance on plug-in systems [1], [2]. In particular, resonant inductive coupling-based systems are preferred due to their higher efficiency at mid-range distances and improved operational safety in practical applications [3]. Recent studies indicate that WPT can also support the widespread adoption of heavy-duty electric commercial vehicles, including buses and trucks, by enabling automated and efficient charging infrastructure [4], [5]. A typical wireless charging system consists of the battery load, rectification and power conversion stages, transmitting and receiving coils, compensation networks, and a high-frequency (HF) inverter [6], [7]. The vehicle battery is charged by converting grid power into high-frequency AC, which is then wirelessly transferred through magnetically coupled coils and rectified, as illustrated in Figure 1.

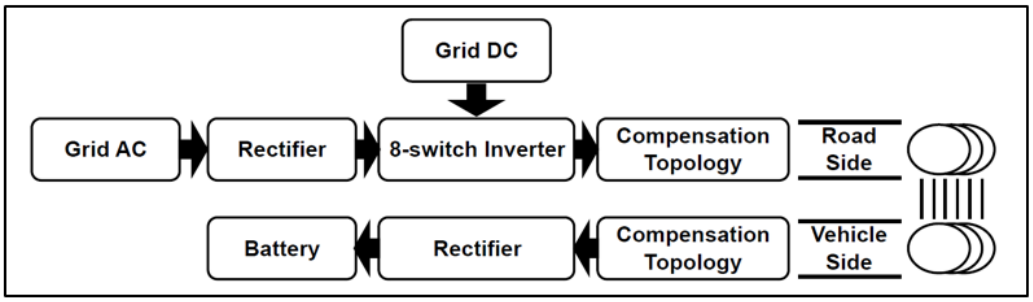

Figure 1. Block diagram of the WPT for EV

In this study, both AC (230 V) and DC (700 V) power-transfer circuits are modeled and analyzed to evaluate performance under coupling coefficients (k) ranging from 0.10 to 0.90 and operating frequencies of 80, 85, and 90 kHz. System behavior is simulated in MATLAB/Simulink, and transient responses are obtained using the fourth-order Runge–Kutta method. Finite-element analysis (FEM) is utilized to verify electromagnetic field interactions and their associated efficiency trends. The aim is to evaluate the AC and DC configurations regarding power-transfer efficiency and stability for heavy-duty electric vehicle applications.

2. LITERATURE REVIEW

WPT has emerged as an essential technology for heavy-duty electric vehicles (HDEVs), as prolonged charging durations and substantial battery capacities present significant challenges. Recent studies have investigated WPT design elements including coil misalignment tolerance, high-power compensation topologies, and efficiency optimization in dynamic conditions. Onar *et al.* [8] developed and empirically validated a 20 kW WPT system for an electric vehicle, showcasing dependable performance within practical limitations. Mou *et al.* [9] examined advancements in magnetic-resonant WPT and emphasized significant circuit enhancements for electric vehicle charging. Deng *et al.* [10] presented an extensive analysis of roadway-powered dynamic wireless charging technologies and their incorporation into transportation infrastructure. Kim *et al.* [11] similarly summarized advancements in power electronics that facilitate high-efficiency inductive charging for electric vehicles. Brownt *et al.* [12] presented a high-power dynamic WPT system exhibiting enhanced tolerance to lateral coil misalignment, demonstrating substantial performance improvements at the vehicle level. Li *et al.* [13] proposed an efficiency-focused control strategy for high-power WPT, optimizing power flow under diverse coupling conditions. Sadar *et al.* [14] performed a comprehensive thermal and cooling analysis of large-capacity battery packs, highlighting thermal stability during elevated charging currents. Notwithstanding these advancements, numerous studies concentrate on discrete subsystems or theoretical conditions, and comprehensive comparisons between AC- and DC-fed WPT architectures, especially those integrating numerical transient modeling with sensitivity analysis, are still scarce. This study offers a system-level comparison of AC and DC WPT configurations through dynamic MATLAB/Simulink modeling and regression analyses to emphasize power transfer efficiency and operational stability.

3. SPECIFIC REQUIREMENTS FOR HEAVY-DUTY VEHICLES

HDEVs impose stringent operational requirements due to their markedly elevated energy demands, prolonged driving ranges, and uninterrupted operational schedules [15]. These vehicles generally necessitate high-capacity battery systems (between 250 kWh and 600 kWh) to guarantee sufficient range and performance across diverse load conditions. Nonetheless, substantial battery capacities present challenges, specifically regarding charging duration, thermal regulation, and overall energy efficiency. These constraints necessitate the development of sophisticated wireless charging solutions that can provide high power while ensuring system stability and safety [15]. TEMSA LD SB E electric bus platform exemplifies these challenges and solutions by integrating a high-capacity lithium-ion battery pack operating at a nominal system voltage of 650 V, optimized for high-power static charging applications [16]. As illustrated in Figure 2, two distinct battery configurations are supported:

- 10-pack layout (2s5p): concentrates battery modules toward the rear axle to enhance traction and maintain optimal load distribution for heavy-duty operation.
- 8-pack layout (2s4p): offers improved weight distribution by shifting a portion of the mass away from the front axle, which enhances handling and vehicle stability under mixed operating conditions.

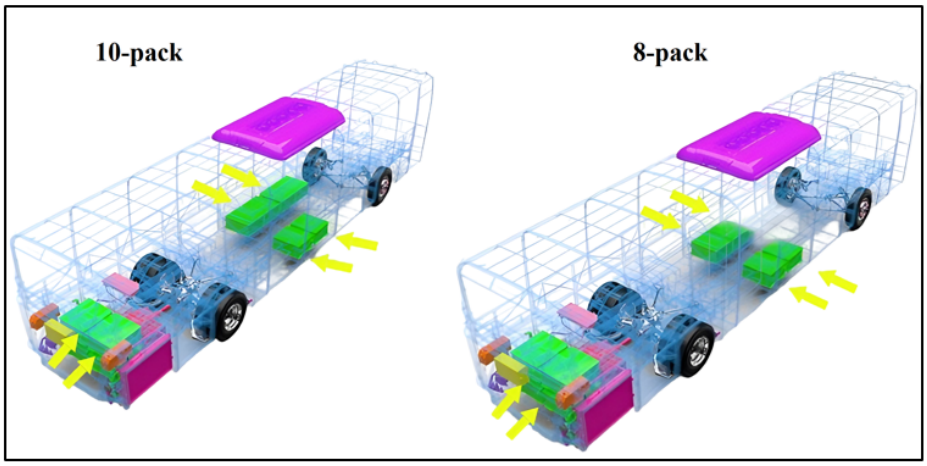

Figure 2. TEMSA LD SB E general layout battery [16]

The 8-pack configuration provides additional flexibility with reduced overall weight, featuring TEMSA TECH battery modules (35 kWh each) with a nominal capacity of 107 Ah, 370 V system voltage, a mass of 255 kg, and 163 liters volume [16]. Thermal management strategies ensure safe operation between -25 °C and 60 °C, with an optimal charging range of 15 °C to 35 °C, power limitation beyond 42 °C, and charge termination at 60 °C. These specifications are vital for the integration of WPT systems in heavy-duty vehicles, where high charging currents and continuous operation amplify the importance of efficient heat dissipation and safe operational margins [16], [17].

4. MATHEMATICAL MODELING OF WIRELESS POWER TRANSFER

WPT system can be represented through an equivalent circuit model to describe energy transfer between the transmitting and receiving coils. This study adopts the series-series (SS) compensation topology, which ensures high efficiency under resonance conditions by maintaining a constant current characteristic [18]. The AC-AC stage of the WPT system is illustrated in Figure 3, where the primary side consists of a voltage source V_1, compensation capacitor C, coil inductance $L_{leak,1}$ and loss resistance R_{loss}. The secondary side includes a similar configuration with coil inductance $L_{leak,2}$ capacitor C, and load impedance Z_L. Magnetic coupling is represented by the mutual inductance L_m while n1:n2 indicates the turns ratio. Accurate evaluation of leakage inductance and resonance frequency is essential for maximizing transfer efficiency. At higher operating frequencies, magnetic coupling is enhanced and losses are reduced, while the coupling coefficient, derived from coil and mutual inductances (M), serves as a key performance indicator:

$$k = \frac{M}{\sqrt{L_1 \times L_2}}$$

where:
- M: mutual inductance
- L_1, L_2: self-inductances of the primary and secondary coils
- k: coupling coefficient $0 \leq k \leq 1$

The coupling coefficient quantifies the fraction of magnetic flux from the primary coil that links with the secondary coil during sinusoidal operation. It is important to note that this definition implicitly assumes stationary, sinusoidal operating conditions, where both coils operate at the same resonant frequency. Under non-sinusoidal or transient excitation, higher-order harmonics may distort the mutual coupling and affect the accuracy of k as parameter [19], making it less representative of actual coupling behavior. The reliance on

sinusoidal waveforms highlights the necessity of developing compensation and control circuits that ensure resonance stability, especially in high-power WPT systems, where waveform distortion may impair coupling and overall efficiency. The resonant frequency for the SS topology is given by:

$$f_0 = \frac{1}{2\pi\sqrt{L \times C}}$$

This condition ensures that the reactance of the compensation capacitors cancels out the inductive reactance of the coils, minimizing reactive power and maximizing real power transfer. Under resonant operation (where the series capacitor reactance cancels the coil reactance), applying Kirchhoff's voltage law (KVL) to the equivalent circuit results in the following differential equations:
Primary side:

$$V_1(t) = R_1 i_1(t) + L_1 \frac{di_1(t)}{dt} + M \frac{di_2(t)}{dt}$$

Secondary side:

$$V_2(t) = R_2 i_2(t) + L_2 \frac{di_2(t)}{dt} + M \frac{di_1(t)}{dt} + v_{\text{load}}(t)$$

where:
- $i_1, i_2(t)$: primary and secondary coil currents
- $v_{\text{load}}(t)$: load-side voltage
- R_1, R_2: coil resistance on each side

These equations define the dynamic behavior of the WPT system and form the basis for evaluating efficiency and voltage/current characteristics under different operating conditions.

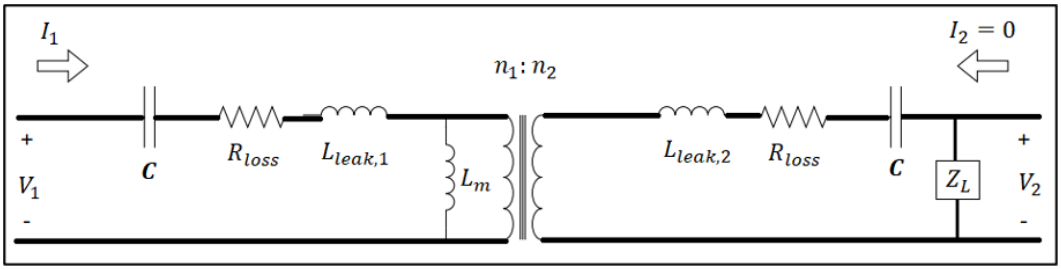

Figure 3. Circuit model of the AC-AC stage of SS WPT topology with the load

5. NUMERICAL ANALYSIS OF WIRELESS POWER TRANSFER SYSTEM

The differential equations presented in section 4 are nonlinear and mutually coupled due to the magnetic coupling between the primary and secondary coils. These equations do not yield closed-form analytical solutions under practical conditions, such as variable coupling coefficients, switching frequencies, and load variations. Therefore, a numerical integration technique is required to simulate system dynamics with high accuracy. The fourth-order Runge-Kutta (RK4) method was chosen because it provides a good balance of computational efficiency and accuracy when solving stiff differential equations in high-frequency power electronic systems [20]. Compared to lower-order methods like Euler or Heun, RK4 has a lower local truncation error while maintaining numerical stability with relatively large step sizes.
The general RK4 algorithm for solving the first-order system:

$$y_{n+1} = y_n + \frac{1}{6} dt(k_1 + 2k_2 + 2k_3 + k_4)$$

with the intermediate slopes calculated as:

$$k_1 = hf(t_n, y_n) - hf\left(t_n + \frac{h}{2}, y_n + \frac{k_1}{2}\right) - hf\left(t_n + \frac{h}{2}, y_n + \frac{k_2}{2}\right) - hf(t_n + h, y_n + k_3)$$

In this case, h represents the step size.

The integration step size h was selected dynamically based on the operating frequency (80–90 kHz) to maintain accurate waveform reconstruction for current and voltage while ensuring numerical stability and precision; smaller step sizes were used for higher frequencies to balance computational efficiency and minimize truncation error without exceeding a maximum error threshold of 0.01%.

To quantify the relationship between input and output power in WPT system, a linear regression model was applied. This approach enables quantifying the predictability and consistency of power transfer under varying operating conditions. The relationship between input power (P_{in}) and output power (P_{out}) can be expressed as:

$$P_{out} = a.P_{in} + b$$

where a represents the slope (indicating power transfer efficiency) and b denotes the constant offset accounting for system losses [21]. For the AC WPT system, the regression model yielded as shown in Figure 4, with:

$$P_{out} = 0.985.P_{in} - 1142.16$$

with a coefficient of determination $R^2 = 0.9919$. This indicates that approximately 99.19% of the variation in output power can be explained by the input power, demonstrating strong linearity but with slightly higher loss components compared to the DC system [22].

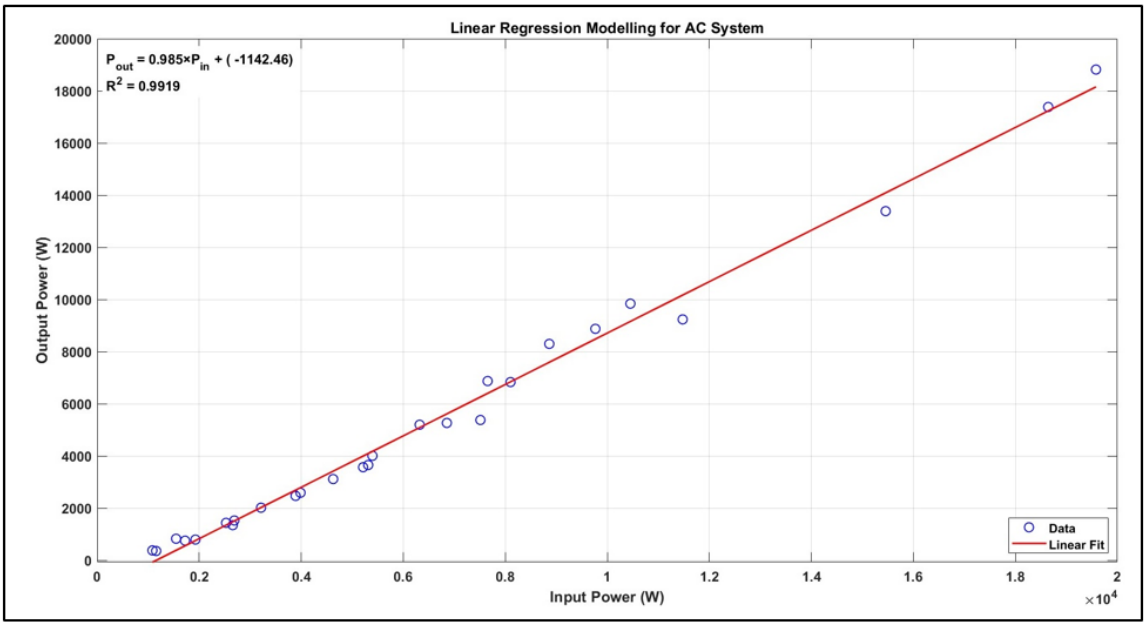

Figure 4. Linear regression modeling for AC system

In contrast, the DC WPT system results are presented in Figure 5, with:

$$P_{out} = 0.959.P_{in} - 2306.40$$

with $R^2 = 0.9892$, signifying robust correlation while suggesting marginally higher non-linearities or losses under certain load conditions. The lower slope reflects the presence of additional energy conversion stages in DC power conditioning, which contributes to minimal efficiency reduction. Overall, both systems demonstrate near-linear power transfer behavior (R^2 >0.98) supporting the predictability of the WPT architectures under the considered operating conditions. However, the AC system exhibited slightly better consistency, while the DC system provided marginally improved robustness at higher power levels [23].

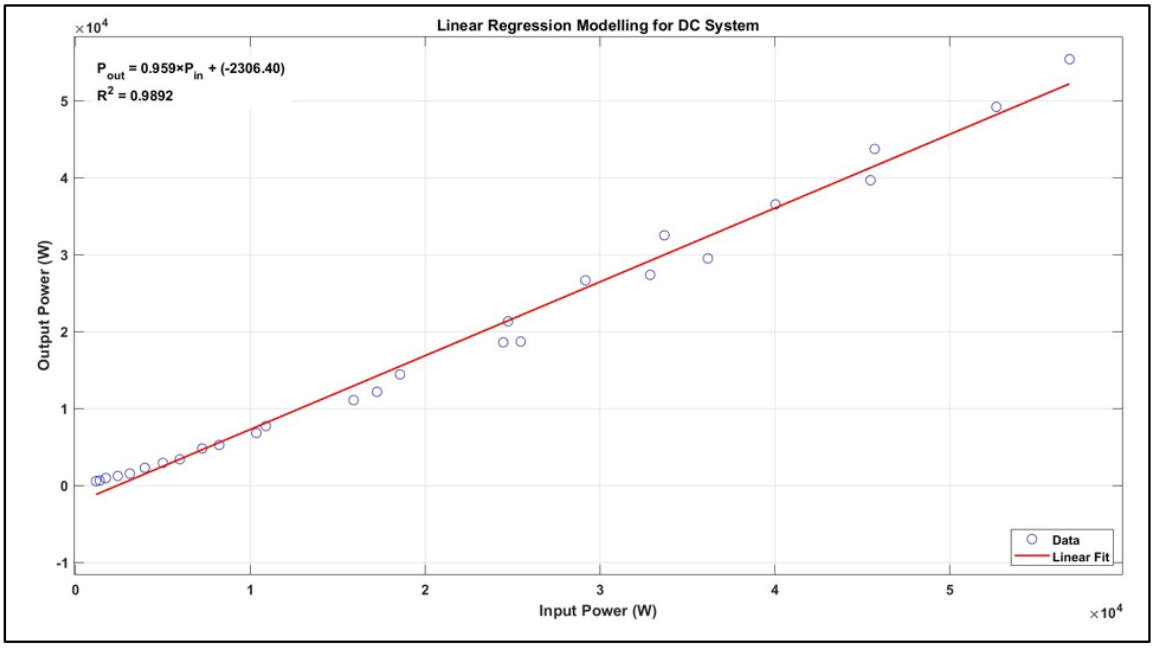

Figure 5. Linear regression modeling for DC system

Residual-based error metrics, namely the root mean square error (RMSE) and mean absolute error (MAE), were evaluated to complement the high R^2 values obtained from the linear regression models. The AC regression yielded RMSE/MAE values of 0.441/0.354 kW with residuals within ± 0.934 kW, while the DC regression yielded RMSE/MAE values of 1.689/1.397 kW with residuals within ± 3.413 kW. It should be noted that these residual-based metrics quantify the fitting accuracy of the linear P_{in}–P_{out} model rather than the conversion loss; therefore, higher efficiency in the DC case does not necessarily imply smaller regression residuals.

System efficiency in WPT systems is highly influenced by variations in coupling coefficient, and operating frequencies. To quantify these effects, sensitivity metrics were computed using normalized derivatives, as defined below:

$$S_f = \frac{\partial \eta}{\partial f} \times \frac{f}{\eta}$$

$$S_k = \frac{\partial \eta}{\partial k} \times \frac{k}{\eta}$$

The terms S_f and S_k refer to how efficiency shifts when we tweak either the operating frequency or the coupling coefficient. To figure these values out, we turned to MATLAB and applied the finite difference method, using simulation data we gathered from different combinations of frequency and coupling. The sensitivity coefficients were determined via finite difference approximation applied to simulation results for AC and DC systems. Normalization ensures that computed values indicate the percentage change in efficiency for a unit percentage change in each parameter. For instance, at 85 kHz, with efficiencies of 96.10% (k=0.90) and 93.22% (k=0.80), the derivative with respect to k yields:

$$\frac{d\eta}{dk} = \frac{93.22 - 96.10}{0.80 - 0.90} = 28.8$$

$$S_k = 28.8 \times \frac{0.85}{94.66} = 0.2586$$

Indicating that a 1% increase in the coupling coefficient results in approximately a 0.26 percentage-point increase in efficiency around the evaluated operating point. This highlights the critical role of coil alignment in

maintaining high performance. The observed sensitivity differences can be explained by how coupling variations affect the power-conditioning stages. In the AC-based resonant architecture, changes in k modify the reflected load and the effective impedance seen by the inverter, which can shift the operating point away from the optimum resonance condition. This detuning increases reactive power circulation and RMS currents in the resonant network, leading to higher copper and switching losses and a steeper efficiency response to coupling variation, especially at low-k conditions. In contrast, the DC-based architecture benefits from the decoupling provided by the rectification and DC/DC regulation stages, where closed-loop control can adjust the conversion ratio and partially compensate power-transfer fluctuations caused by coupling changes.

As a result, the DC system exhibits smoother trends and reduced sensitivity under the tested operating range. To provide a first-order robustness indicator, Figure 6 includes variability bars for the representative 85 kHz case by assuming a coupling tolerance of $\Delta k = \pm 0.02$ and propagating it to the corresponding variation in S_k. From a design perspective, these results imply that AC-resonant WPT systems require tighter resonance management (e.g., frequency tracking or adaptive tuning) to remain robust against misalignment and k-variation, whereas DC-based solutions can tolerate wider coupling variations but must still account for additional conversion-stage losses and control limits under weak coupling [24], [25].

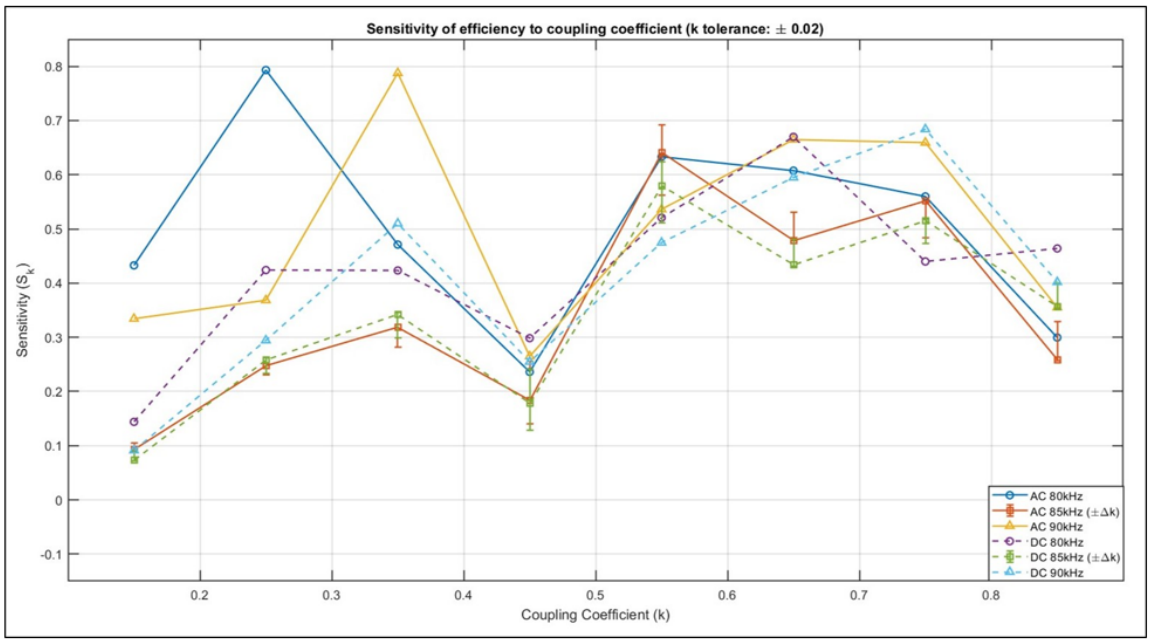

Figure 6. Sensitivity of efficiency to coupling coefficient

6. SIMULATION FRAMEWORK FOR AC AND DC SYSTEMS

The simulation framework was developed in MATLAB/Simulink to compare AC and DC WPT configurations for HDEV charging. Both systems were simulated over a coupling coefficient range of $0.10 \leq k \leq 0.90$ and at resonant frequencies of 80, 85, and 90 kHz. The AC configuration assumes a 230 V RMS input and employs an eight-switch inverter with sinusoidal PWM to generate the high-frequency excitation, followed by an series–series (SS) compensation network [26]. The DC configuration operates with a regulated 700 V DC bus at the input stage, eliminating the grid-side rectification stage present in the AC input case. At the receiver side, the induced AC is rectified to supply the battery. Figure 7 shows the combined Simulink representations of the AC and DC WPT systems.

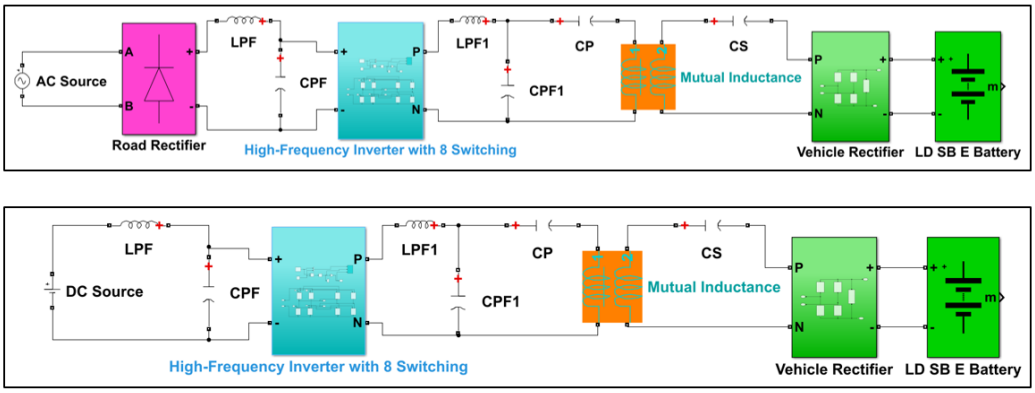

Figure 7. Simulink model of the AC and DC WPT system for LD SB E

Both systems implemented an eight-switch inverter topology (H1–H8), as shown in Figure 8, which offers enhanced control flexibility compared to the conventional four-switch design [27]. Complementary PWM signals were used to operate the switches in pairs, generating high-frequency AC with reduced harmonic distortion. This design ensured precise waveform shaping and improved conversion efficiency.

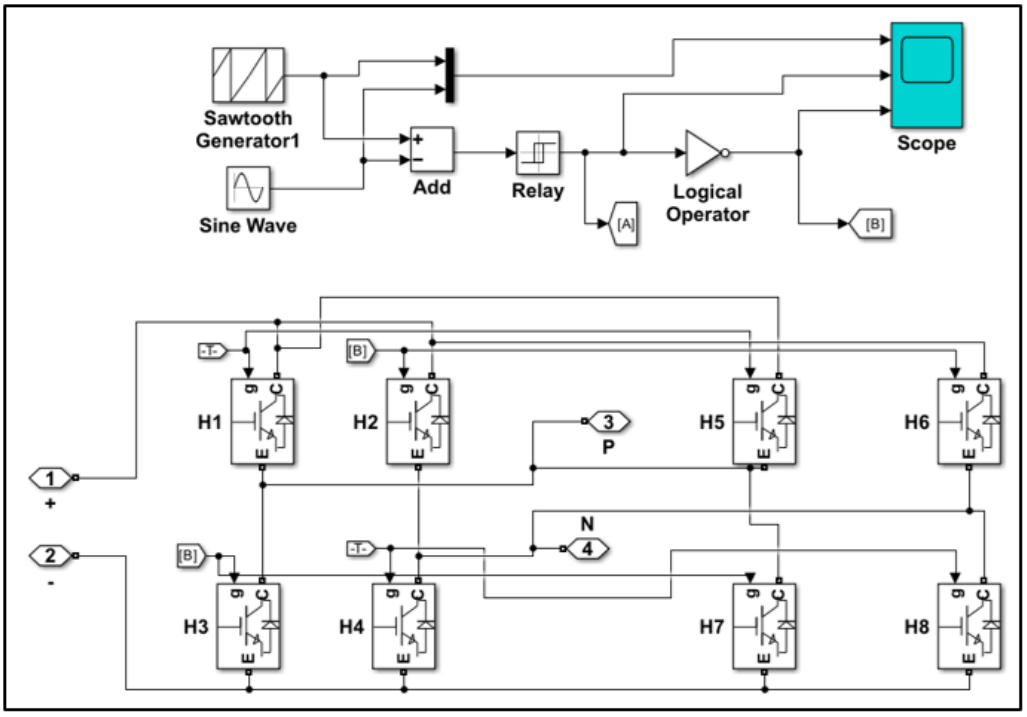

Figure 8. High-frequency inverter with 8 switching elements for AC and DC WPT system

At 85 kHz and coupling coefficient of 0.90, the eight-switch inverter achieved 96.10% efficiency versus 94.8% for the four-switch baseline, corresponding to a +1.30 percentage-point improvement. Equivalently, the loss fraction decreased from 5.20% to 3.90%, which corresponds to an approximately 25% relative reduction at this operating point.

The PWM generation process for the inverter is further illustrated in Figure 9, which displays the carrier and reference waveforms, the result of PWM pulses, and their logical complements. These signals regulate the switching elements in pairs, ensuring efficient inverter operation with reduced harmonic content [28].

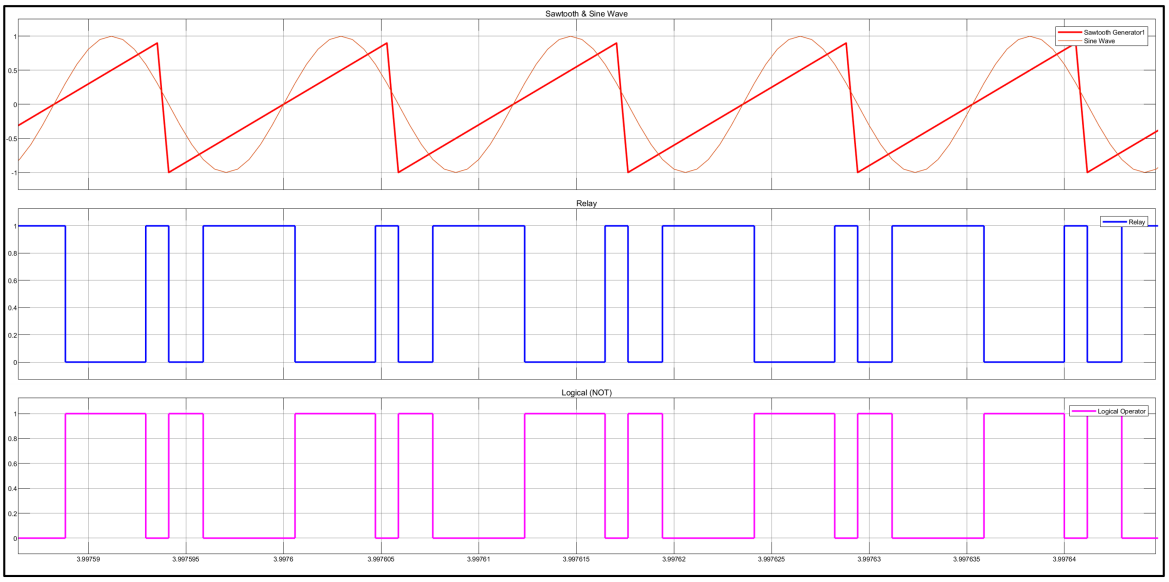

Figure 9. Switching signal generation process in the HF inverter

Figure 10 depicts the full-bridge rectification of the AC signal generated in the secondary coil on the receiver side. This circuit, engineered for compatibility with both AC and DC inputs, reduced voltage ripple and stabilized the charging current. The rectifier, in conjunction with an output capacitor, established secure charging parameters for the 652 V/280 kWh LD SB E battery pack [16].

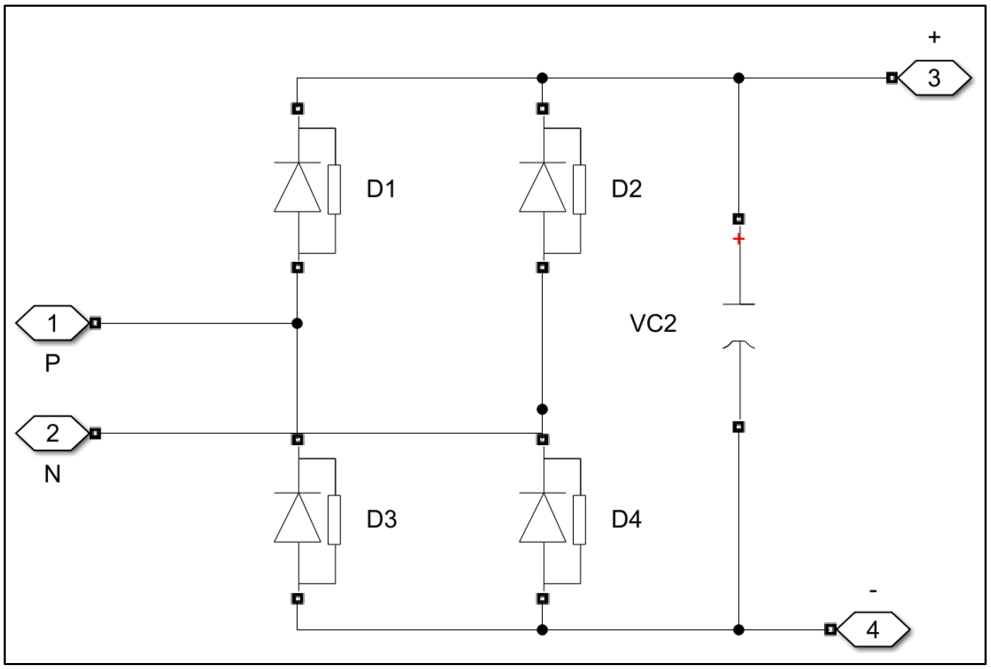

Figure 10. Vehicle rectifier for AC and DC WPT system

Simulations were conducted at 85 kHz with a coupling coefficient of 0.90 to validate the performance of the AC-based WPT system, representing the highest recorded efficiency scenario. Figure 11 depicts the input voltage and current waveforms, both demonstrating distinct sinusoidal patterns, thereby affirming stable resonance and effective energy transfer from the grid.

The corresponding active input power rapidly stabilizes after a short transient period, as shown in Figure 12, indicating reliable operation under these optimal conditions.

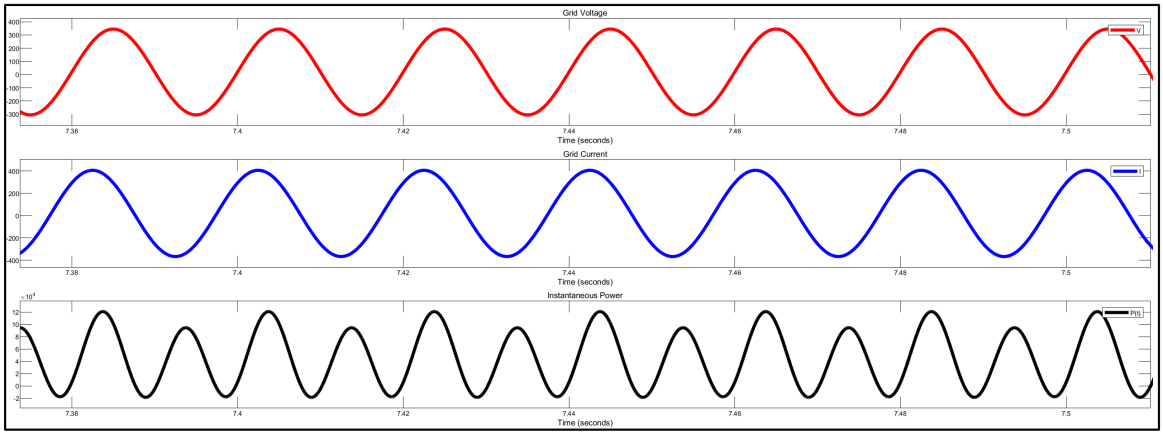

Figure 11. Input voltage and current waveforms at 85 kHz and k = 0.90

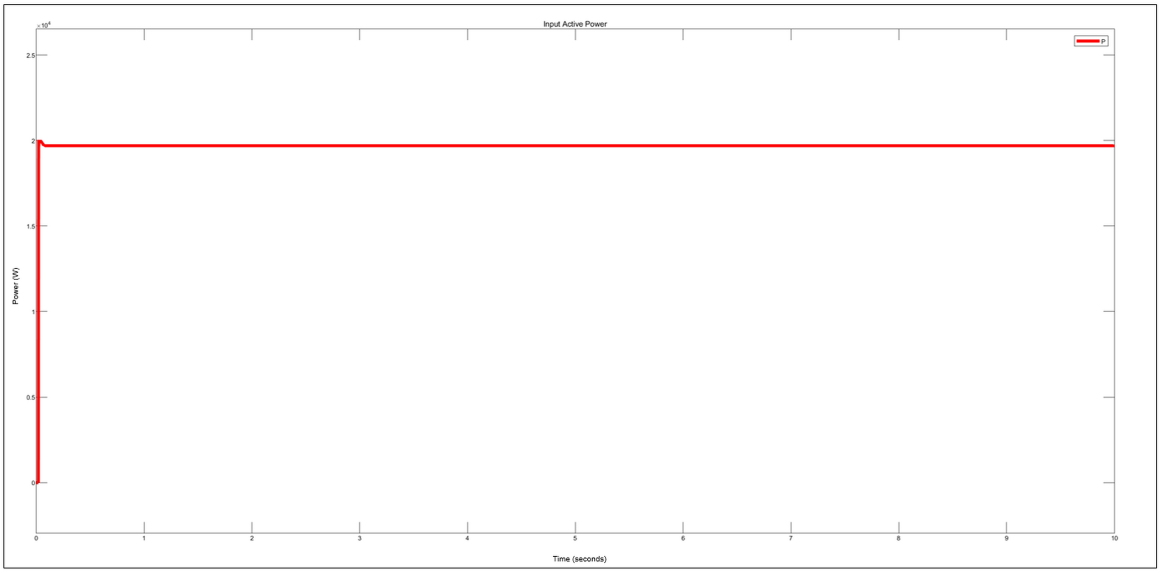

Figure 12. Input active power waveforms at 85 kHz and k = 0.90

Both the transmitter and receiver exhibit stable and sinusoidal characteristics in their winding voltage and current waveforms, as depicted in Figure 13. The roadside coil's waveforms display elevated amplitudes, indicating effective magnetic induction and negligible energy losses in the resonant circuit. In contrast, the vehicle-side winding exhibits diminished amplitudes owing to intrinsic coil-to-coil transfer properties, while maintaining a distinct sinusoidal form. The symmetry and stability validate adequate energy coupling and minimal distortion, guaranteeing that most transmitted energy is efficiently delivered to the load. The findings further confirm the resilience of the SS compensation topology under optimal operating conditions, facilitating efficient coil-to-coil power transmission and enhancing system performance [29], [30].

The battery response is presented in Figure 14, which shows battery voltage, current, and state of charge (SoC). After a brief stabilization, the battery voltage and current remain steady, and SoC increases continuously, confirming a robust and consistent charging process.

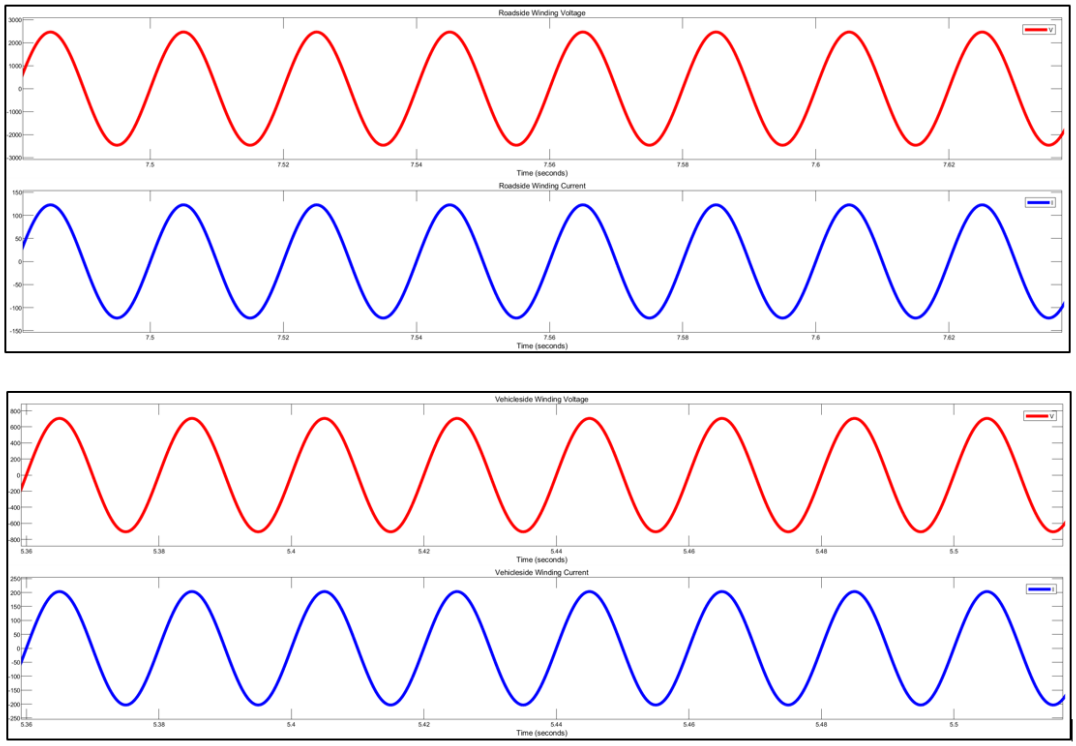

Figure 13. Road and vehicleside winding voltage and current at 85 kHz and k = 0.90

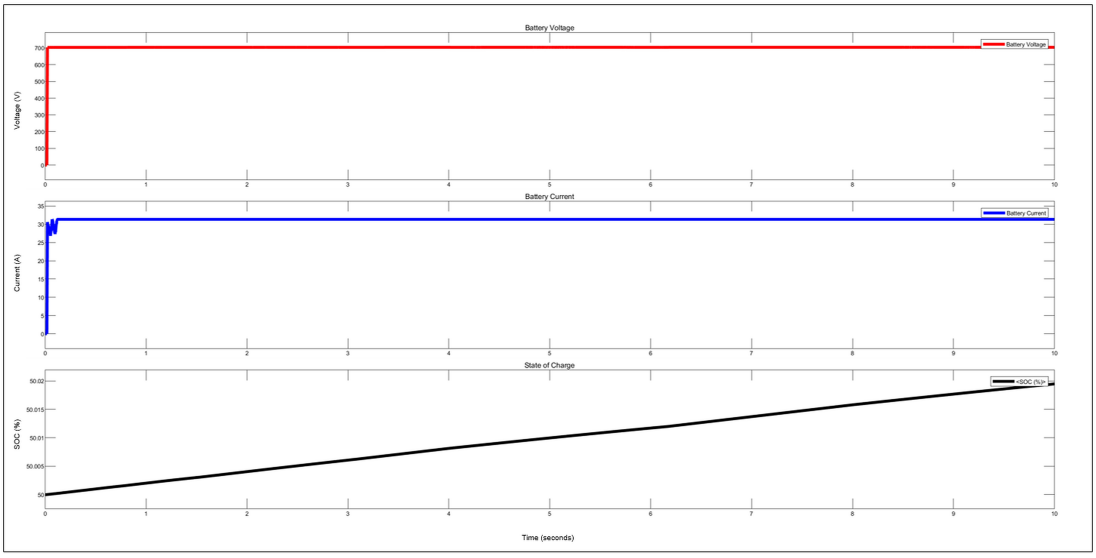

Figure 14. Battery voltage, current, and SoC at 85 kHz and k = 0.90

The associated battery power and cumulative energy are shown in Figure 15, demonstrating sustained energy transfer over time.

Finally, Figure 16 shows the capacitor voltages and currents on the primary and secondary sides. A distinct 90° phase shift between current and voltage is observed, which is the key characteristic of the SS compensation topology, minimizes reactive power circulation and ensures maximum real power transfer. The findings validate that the AC system attains over 96% efficiency, aligning with earlier published results [31], [32] that illustrate the efficacy of resonant WPT topologies for high-power applications.

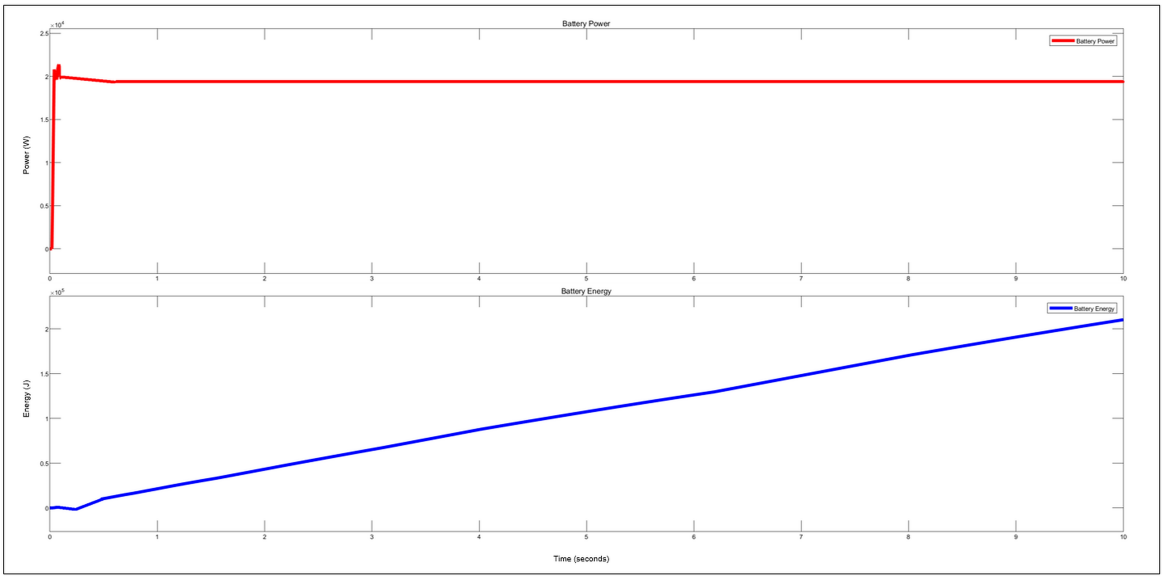

Figure 15. Battery power and energy at 85 kHz and k = 0.90

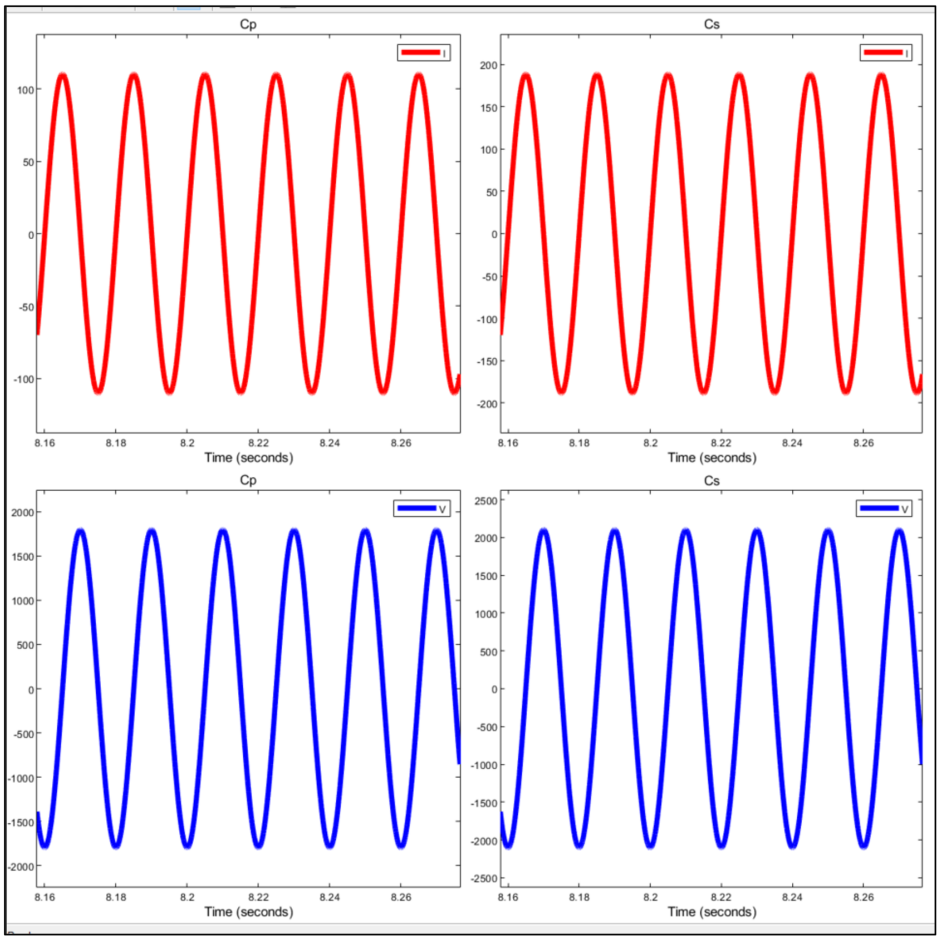

Figure 16. Primary and secondary capacitor currents and voltages at 85 kHz and k = 0.90

Table 1 summarizes the AC WPT simulation results across the considered operating conditions, reporting input/output powers, transferred energy, and efficiency. The results show that AC efficiency is highly sensitive to coupling: the maximum efficiency reaches 96.10% at 85 kHz and $k = 0.90$, whereas it drops to 30.82% at 80 kHz and $k = 0.10$. Overall, stronger coupling yields higher and more stable power transfer, while weak coupling significantly degrades AC-system performance [33], [34].

Table 1. Summary of simulation results for AC WPT systems

No	Grid (AC) (V)	Frequency (kHz)	Coupling coefficient	Input power (W)	Primary power (W)	Secondary power (W)	Output power (W)	Energy (J)	Efficiency (%)
1	230	80	0.90	10452.97	10427.97	10426.07	9839.35	98679.20	94.13
2	230	80	0.50	5213.45	4983.45	4953.45	3568.33	35326.47	68.44
3	230	80	0.10	1156.22	934.84	844.46	356.32	3767.19	30.82
4	230	85	0.90	19580.13	19490.18	19486.31	18815.80	210338.71	96.10
5	230	85	0.50	7512.45	6312.15	6254.15	5378.69	51904.36	71.60
6	230	85	0.10	1546.92	1523.11	1439.85	826.18	8647.58	53.41
7	230	90	0.90	8862.83	8841.67	8840.21	8296.64	80091.45	93.61
8	230	90	0.50	4625.66	4588.55	4537.90	3114.05	28960.67	67.32
9	230	90	0.10	1082.78	865.97	844.59	378.07	3436.50	34.92

Table 2 presents the DC WPT simulation results for 80–90 kHz and $k = 0.10$–0.90, including input/output powers, transferred energy, and efficiency. Compared with the AC case, the DC configuration maintains higher efficiency and better robustness, especially at strong coupling; the maximum efficiency reaches 97.44% at 85 kHz and $k = 0.90$. Overall, the DC architecture provides more stable performance across frequency variations, supporting its suitability for high-power charging scenarios [35], [36].

Table 2. Summary of simulation results for DC WPT systems

No	Grid (DC) (V)	Frequency (kHz)	Coupling coefficient	Input power (W)	Primary power (W)	Secondary power (W)	Output power (W)	Energy (J)	Efficiency (%)
1	700	80	0.90	33671.68	33498.09	33490.77	32511.66	324356.67	96.55
2	700	80	0.50	10876.44	10822.49	10743.19	7703.58	75649.16	70.83
3	700	80	0.10	1379.41	1316.52	1234.79	619.90	6884.11	44.94
4	700	85	0.90	56840.76	56418.51	56389.48	55386.71	513732.19	97.44
5	700	85	0.50	25457.66	25362.44	25271.90	18694.43	176101.53	73.43
6	700	85	0.10	1726.11	1699.51	1614.72	948.47	9143.50	54.95
7	700	90	0.90	45696.29	45458.91	45447.80	43721.63	426285.89	95.68
8	700	90	0.50	15898.51	15818.21	15732.08	11085.10	108633.98	69.72
9	700	90	0.10	1163.45	1075.69	1031.61	553.95	5605.97	47.61

Table 3 presents first-order theoretical estimates of the charging time required to increase the battery SoC from 20% to 80% for a 280 kWh battery under the constant average output power assumption ($\Delta E = 168$ kWh). Based on the simulation results, the AC configuration yields estimated charging times ranging from 8.93 to 20.24 h across the 80–90 kHz frequency range due to frequency-dependent resonant behavior, whereas the DC configuration reduces this duration to 3.03–5.17 h under the same coupling coefficient, indicating a significantly shorter charger occupancy for the DC case.

Table 3. Estimated charging time for 20–80% SoC (280 kWh battery), $k = 0.90$

No	Grid	Frequency (kHz)	Coupling coefficient	Charging time (h)
1	AC	80	0.90	17.07
2	AC	85	0.90	8.93
3	AC	90	0.90	20.24
4	DC	80	0.90	5.17
5	DC	85	0.90	3.03
6	DC	90	0.90	3.84

7. CONCLUSION

This study compared AC- and DC-based WPT architectures for heavy-duty electric vehicle charging using MATLAB/Simulink, supported by regression and sensitivity analyses. Peak efficiencies of 96.10% for the AC configuration and 97.44% for the DC configuration were achieved at 85 kHz and a coupling coefficient of $k = 0.90$. Overall, the DC topology demonstrated more stable performance, lower sensitivity to parameter variations, and more consistent charging behavior, confirming its suitability for high-power applications. However, the analysis was limited to simulation-based evaluation under idealized operating conditions without detailed thermal modeling, electromagnetic field effects, or experimental validation. Future work will focus on hardware implementation, investigation of coil misalignment and thermal effects, and optimization of converter control strategies to further enhance system efficiency and robustness under practical operating conditions.

ACKNOWLEDGMENTS

The authors would like to thank TEMSA Skoda Sabancı Ulaşım SAN.TİC.A.Ş. for their valuable support and contributions throughout this research.

FUNDING INFORMATION

The authors state no funding involved.

AUTHOR CONTRIBUTIONS STATEMENT

This journal uses the Contributor Roles Taxonomy (CRediT) to recognize individual author contributions, reduce authorship disputes, and facilitate collaboration.

Name of Author	C	M	So	Va	Fo	I	R	D	O	E	Vi	Su	P	Fu
Mustafa Karavuş	✓	✓	✓	✓	✓	✓		✓	✓	✓	✓			
Ahmet Arif Ergin	✓	✓			✓					✓		✓	✓	
Gulten Polat				✓	✓	✓				✓				
Bünyamin Eşiyok	✓				✓	✓				✓				

C : **C**onceptualization
M : **M**ethodology
So : **So**ftware
Va : **Va**lidation
Fo : **Fo**rmal Analysis
I : **I**nvestigation
R : **R**esources
D : **D**ata Curation
O : Writing - **O**riginal Draft
E : Writing - Review & **E**diting
Vi : **Vi**sualization
Su : **Su**pervision
P : **P**roject Administration
Fu : **Fu**nding Acquisition

CONFLICT OF INTEREST STATEMENT

Authors state no conflict of interest.

DATA AVAILABILITY

The data that support the findings of this study are available from the corresponding author, Mustafa Karavuş, upon reasonable request.

REFERENCES

[1] E. Aydin, M. T. Aydemir, A. Aksoz, M. El Baghdadi, and O. Hegazy, "Inductive Power Transfer for Electric Vehicle Charging Applications: A Comprehensive Review," *Energies*, vol. 15, no. 14, pp. 1-24, 2022, doi: 10.3390/en15144962.

[2] J. Jiang, X. Zhou, Y. Li, Z. Yu, and W. Gu, "Frequency Stability Analysis and Charging Area Expansion of Matrix-Coupled Wireless Power Transfer," *Electronics*, vol. 13, no. 7, pp. 1-20, 2024, doi: 10.3390/electronics13071312.

[3] W. Niu, J. Jiang, C. Ye, and W. Gu, "Frequency Splitting Suppression in Wireless Power Transfer Using Hemispherical Spiral Coils," *AIP Advances*, vol. 12, no. 5, 2022, doi: 10.1063/5.0078744.

[4] N. T. Diep and N. K. Trung, "Transmitting Side Power Control for Dynamic Wireless Charging System of Electric Vehicles," *Engineering, Technology & Applied Science Research*, vol. 12, no. 4, pp. 9042-9047, 2022, doi: 10.48084/etasr.4988.

[5] S. Liu, X. Yan, G. Xu, G. Wang, and Y. Liu, "An Eight-Coil Wireless Power Transfer Method for Improving the Coupling Tolerance Based on Uniform Magnetic Field," *Processes*, vol. 12, no. 10, pp. 1-13, 2024, doi: 10.3390/pr12102109.

[6] I. Okasili, A. Elkhateb, and T. Littler, "A review of wireless power transfer systems for electric vehicle battery charging with a focus on inductive coupling," *Electronics*, vol. 11, no. 9, pp. 1-26, 2022, doi: 10.3390/electronics11091355.

[7] SAE International, "Wireless Power Transfer for Heavy-Duty Electric Vehicles," SAE Standard J2954/2_202212, 2022, doi: 10.4271/J2954/2_202212.

[8] O. C. Onar, M. Chinthavali, S. L. Campbell, L. E. Seiber, C. P. White, and V. P. Galigekere, "Modeling, Simulation, and Experimental Verification of a 20-kW Series-Series Wireless Power Transfer System for a Toyota RAV4 Electric Vehicle," in *2018 IEEE Transportation Electrification Conference and Expo (ITEC)*, Long Beach, CA, USA, 2018, pp. 436–441, doi: 10.1109/ITEC.2018.8450085.

[9] X. Mou, D. T. Gladwin, R. Zhao, and H. Sun, "Survey on magnetic resonant coupling wireless power transfer technology for electric vehicle charging," *IET Power Electronics*, vol. 12, no. 12, pp. 3005–3020, 2019, doi: 10.1049/iet-pel.2019.0529.

[10] B. Deng, B. Jia, and Z. Zhang, "Dynamic Wireless Charging for Roadway-Powered Electric Vehicles: A Comprehensive Analysis and Design," *Progress In Electromagnetics Research C*, vol. 69, pp. 1–10, 2016, doi: 10.2528/PIERC16071106.

[11] S. Kim, G. A. Covic, and J. T. Boys, "Tripolar pad for inductive power transfer systems for EV charging," *IEEE Transactions on Power Electronics*, vol. 32, no. 7, pp. 5045–5057, 2017, doi: 10.1109/TPEL.2016.2606893.

[12] A. D. Brownt, D. Aliprantis, S. D. Pekarek, A. Agostino, and D. Haddad, "Design and analysis of a three-phase dynamic wireless power transfer system for heavy-duty electric vehicles considering misalignment," in *2022 Wireless Power Week (WPW)*, Bordeaux, France, 2022, pp. 867-872, doi: 10.1109/WPW54272.2022.9901341.

[13] J. Li, J. Wang, J. Li, and J. Chen, "Multivariable coordinated control strategy for efficiency optimization without real-time wireless feedback communication in wireless power transfer," *IEEE Access*, vol. 10, pp. 55381–55395, 2022, doi: 10.1109/ACCESS.2022.3174122.

[14] A. Sadar, M. Alqahtani, and N. Mohammad, "An optimal design of battery thermal management system with advanced heating and cooling control mechanism for lithium-ion storage packs in electric vehicles," *Journal of Energy Storage*, vol. 101, 2024, doi: 10.1016/j.est.2024.113421.

[15] J. M. Miller and A. Daga, "Elements of wireless power transfer essential to high power charging of heavy duty vehicles," *IEEE Transactions on Transportation Electrification*, vol. 1, no. 1, pp. 26–39, 2015, doi: 10.1109/TTE.2015.2426500.

[16] TEMSA R&D Department, "LD SB E Electric Bus Platform: Internal Technical Specifications," TEMSA Skoda Sabancı Global A.Ş., Adana, Turkey, Tech. Rep., 2025.

[17] BSI, Electric vehicle wireless power transfer (WPT) systems—Part 5: Interoperability and safety of dynamic wireless power transfer (D-WPT) for electric vehicles, BSI Standards Publication, 2024, doi: 10.3403/30506653.

[18] C. T. Rim and C. Mi, *Wireless Power Transfer for Electric Vehicles and Mobile Devices*. Hoboken, NJ, USA: Wiley, 2017, doi: 10.1002/9781119329084.

[19] S. G. Cimen and B. Schmuelling, "A dynamic model of the bidirectional inductive power transfer system for electric vehicles," in *2014 16th European Conference on Power Electronics and Applications*, Lappeenranta, Finland, 2014, doi: 10.1109/EPE.2014.6910996.

[20] J. C. Butcher, *Numerical Methods for Ordinary Differential Equations*, 3rd ed. Chichester, UK: Wiley, 2016, doi: 10.1002/9781119121534.

[21] D. C. Montgomery, E. A. Peck, and G. G. Vining, *Introduction to Linear Regression Analysis*, 6th ed. Hoboken, NJ, USA: Wiley, 2021.

[22] D. Chicco, M. J. Warrens, and G. Jurman, "The coefficient of determination R-squared is more informative than SMAPE, MAE, MAPE, MSE and RMSE in regression analysis evaluation," *PeerJ Computer Science*, vol. 7, Art. no. e623, 2021, doi: 10.7717/peerj-cs.623.

[23] M. Vinod, D. Kishan, and B. Reddy, "Three-leg DC–DC converter for efficient inductive power transfer of electric vehicles for wide-range battery applications," *IEEE Transactions on Power Electronics*, vol. 38, no. 8, pp. 10079–10091, 2023, doi: 10.1109/TPEL.2023.3269886.

[24] S. Jiao, S. Li, J. Wu, L. Wang, and J. Li, "Maximizing energy efficiency for wireless power transfer systems through an optimal frequency control strategy," in *2024 IEEE Wireless Power Technology Conference and Expo (WPTCE)*, Kyoto, Japan, 2024, doi: 10.1109/WPTCE59894.2024.10557389.

[25] R. Qin, J. Li, J. Sun, and D. Costinett, "Shielding design for high-frequency wireless power transfer system for EV charging with self-resonant coils," in *2022 IEEE Energy Conversion Congress and Exposition (ECCE)*, Detroit, MI, USA, 2022, pp. 1–8, doi: 10.1109/ECCE50734.2022.9948194.

[26] Y. Chen, H. Zhang, S.-J. Park, and D.-H. Kim, "A comparative study of S-S and LCCL-S compensation topologies in inductive power transfer systems for electric vehicles," *Energies*, vol. 12, no. 10, pp. 1-19, 2019, doi: 10.3390/en12101913.

[27] E. Chaidee, A. Sangswang, S. Naetiladdanon, and S. Nutwong, "An inverter topology for multitransmitter wireless power transfer systems," *IEEE Access*, vol. 10, pp. 36592–36605, 2022, doi: 10.1109/ACCESS.2022.3162906.

[28] K. Thiagarajan and T. Deepa, "A comprehensive review of high-frequency transmission inverters for magnetic resonance inductive wireless charging applications in electric vehicles," *IETE Journal of Research*, vol. 69, no. 5, pp. 2761–2771, 2023, doi: 10.1080/03772063.2021.1905089.

[29] K. Song, Z. Li, J. Jiang, and C. Zhu, "Constant current/voltage charging operation for series–series and series–parallel compensated wireless power transfer systems employing primary-side controller," *IEEE Transactions on Power Electronics*, vol. 33, no. 9, pp. 8065–8080, 2018, doi: 10.1109/TPEL.2017.2767099.

[30] Y. Gao, A. Ginart, K. B. Farley, and Z. T. H. Tse, "Misalignment effect on efficiency of wireless power transfer for electric vehicles," in *2016 IEEE Applied Power Electronics Conference and Exposition (APEC)*, Long Beach, CA, USA, 2016, pp. 3526–3528, doi: 10.1109/APEC.2016.7468375.

[31] R. Qin, J. Li, and D. Costinett, "A 6.6-kW high-frequency wireless power transfer system for electric vehicle charging using multilayer nonuniform self-resonant coil at MHz," *IEEE Transactions on Power Electronics*, vol. 37, no. 4, pp. 4842–4856, 2022, doi: 10.1109/TPEL.2021.3120734.

[32] Md Aurongjeb, Y. Liu, and M. Ishfaq, "Design and simulation of inductive power transfer pad for electric vehicle charging," *Energies*, vol. 18, no. 2, pp. 1-13, 2025, doi: 10.3390/en18020244.

[33] Z. Yao and Y. Zhang, "Variable structure wireless power transfer converter with misalignment tolerant," *International Journal of Electrical Power & Energy Systems*, vol. 170, pp. 1-15, 2025, doi: 10.1016/j.ijepes.2025.110967.
[34] R. Matsumoto and H. Fujimoto, "Wireless EV charging system using PWM-controlled variable capacitor for maximum power transfer under severe coil misalignment," in *2022 International Power Electronics Conference (IPEC-Himeji 2022-ECCE Asia*, Himeji, Japan, 2022, pp. 1476–1481, doi: 10.23919/IPEC-Himeji2022-ECCE53331.2022.9806942.
[35] D. Kishan, B. Mallikarjuna, M. W. Ahmad, and A. Chub, "Design of a multi-mode DC–DC converter for high-power wireless charging of electric vehicles," in *2024 IEEE International Conference on Power Electronics, Drives and Energy Systems (PEDES)*, Mangalore, India, 2024, pp. 1–6, doi: 10.1109/PEDES61459.2024.10961040.
[36] Z. Deng, S. Zhang, G. Zhu, J. Dong, Y. Li, and P. Bauer, "Direct matrix converter-based modular high-power wireless charging systems for heavy-duty electric vehicles," *IEEE Journal on Wireless Power Technologies*, 2026, doi: 10.1109/JWPT.2026.3670766.

BIOGRAPHIES OF AUTHORS

Mustafa Karavuş was born in Istanbul, Turkey, in 1996. He received his B.Sc. degree in Electrical and Electronics Engineering from Yeditepe University, Istanbul, Turkey, in 2022, and his M.Sc. degree in Electrical and Electronics Engineering from Yeditepe University in 2025. He is currently working as a Technical Specialist at TEMSA Skoda Sabancı Ulaşım SAN.TİC.A.Ş. His research interests include wireless power transfer systems, electric motors, transformers, battery management systems, magnetic field analysis, and power electronics. He can be contacted at email: mustafa.karavus@std.yeditepe.edu.tr and mustafa.karavus@temsa.com.

Prof. Dr. Ahmet Arif Ergin is a Professor in the Department of Electrical and Electronics Engineering and currently serves as the Dean of the Faculty of Engineering at Bahçeşehir University, Istanbul, Turkey. He received his B.Sc. degree in Electrical and Electronics Engineering from Middle East Technical University (METU) in 1992, and his M.Sc. and Ph.D. degrees in Electrical and Computer Engineering from the University of Illinois at Urbana-Champaign in 1995 and 2000, respectively. His research interests include electromagnetic fields and microwave techniques, and advanced algorithms for time-domain analysis of electromagnetic wave phenomena. He has contributed significantly to the field through his research on three-dimensional transient wave phenomena, marching-on-in-time solution methods, and scattering from conducting strips, utilizing both theoretical and computational approaches. He can be contacted at email: arif.ergin@bau.edu.tr.

Assoc. Dr. Gulten Polat is an Associate Professor in the Department of Civil Engineering at Yeditepe University, Istanbul, Turkey. She received her B.Sc. degree in Geophysics Engineering from Dokuz Eylul University in 2000 and holds two Ph.D. degrees in Geophysics: from University College Dublin (2014) and Boğaziçi University (2019). Her research interests encompass geophysics and geology, with a focus on local earthquake tomography, seismic velocity structures (P- and S-waves), seismic anisotropy, and tectonic characterization of Ireland and Turkey. She is also engaged in the analysis and modelling of complex, multidisciplinary datasets, applying advanced numerical and statistical techniques to geophysical and broader scientific data. She can be contacted at email: gulten.polat@yeditepe.edu.tr.

Dr. Bünyamin Eşiyok is an electrical and electronics engineer currently working as a part-time academic at Yeditepe University in Istanbul, where he teaches undergraduate courses and contributes to various academic activities. He completed his Ph.D. in 2024 at Yeditepe University, with a focus on intelligent vehicle technologies. His academic interests include electric vehicles, autonomous systems, machine learning applications, and control engineering. In addition to his teaching responsibilities, he is involved in industry-related projects and provides consultancy services, particularly in the field of automotive technologies. He teaches undergraduate level courses on intelligent vehicles, vehicle electrification, fundamentals of programming, and electrical circuits. He can be contacted at email: bunyamin.esiyok@yeditepe.edu.tr.